Lasers in Manufacturing Conference 2023

Fabrication of an athermal mirror from a hyper-eutectic AlSi alloy via LPBF

Christoph Wilsnack[a,*], Juliane Moritz[a], Arnd Reutlinger[b], Sebastian Eberle[b], Lukas Stepien[a], Elena Lopez[a], Frank Brückner[a,d], Christoph Leyens[a,c]

[a]*Fraunhofer Institute for Material and Beam Technology, Dresden, 01277, Germany*
[b]*Kampf Telescope Optics GmbH, Munich, 81379, Germany*
[c]*Technische Universität Dresden, Dresden, 01069, Germany*
[d]*Luleå University of Technology, Luleå, 971 87, Sweden*

Abstract

This study explores the use of a combination of the hypereutectic aluminum-silicon alloy AlSi40 and electroless nickel (NiP) for optical mirrors in space-borne instruments. The combination of AlSi40 and NiP offers a solution to the trade-offs between optical performance, structural integrity, manufacturing time and price that traditional materials used for optical space applications have. AlSi40 is processable by additive technologies like Laser Powder Bed Fusion (LPBF), which allows the design and fabrication of optical components with optimized internal structures (e.g. lattice structures) resulting in increased stiffness-to-mass ratio of the component, which is crucial for space applications. The process chain, including parameter development and material characterization, was conducted and a demonstrator mirror was printed and tested under representative operational conditions. The study also includes the transfer process of the parameters and the experimental conditions between several AM machines, to ensure the scalability and reproducibility of the process.

Keywords: Laser Powder Bed Fusion; Additive Manufacturing; Quality Assurance; Space; AlSi40; hyper-eutectic alloy

1. Introduction

Optical mirrors used in space-based optical instruments are subjected to extreme mechanical stresses during the launch phase and must also perform reliably under significant temperature variations in orbit. Materials selected for optical applications in space typically include metals, ceramics, and glass-ceramics, each presenting a challenging trade-off between optical performance, structural integrity, manufacturing efficiency, and cost. Glass and ceramics are known for their suitability in achieving highly precise optical surfaces, but they often lack the necessary structural robustness. On the other hand, metals like aluminum offer high

strength and specific stiffness but fall short in providing optical surfaces with extremely low roughness (Jenzer *et al.*, 2017).

To address these challenges, a promising approach emerges, which involves combining the benefits of an aluminum-silicon alloy, specifically the hypereutectic AlSi40, with a hard coating such as electroless nickel (NiP) to achieve high precision optical surfaces. The combination of these materials is particularly appealing for athermal mirrors in space-based optical instruments, as both exhibit a closely matched coefficient of thermal expansion (CTE). This characteristic mitigates the occurrence of bi-metallic bending effects during temperature fluctuations, making this combination highly attractive for space applications (Ma *et al.*, 2014).

Furthermore, the utilization of AlSi40 presents an additional advantage in terms of its processability through additive technologies. Additive manufacturing techniques, notably Laser Powder Bed Fusion (LPBF), enable the design and fabrication of optical components with optimized internal structures, such as lattice structures. These internal structures enhance the stiffness-to-mass ratio of the component, a crucial factor for space applications where weight reduction is essential (Hilpert *et al.*, 2019).

To explore the potential of the AlSi40 alloy coated with electroless nickel (NiP) as a viable solution for spaceborne optical mirrors the mechanical performance under launch conditions and its optical performance within the demanding thermal variations experienced in orbit must be investigated and evaluated. Additionally, the advantages offered by additive manufacturing techniques, specifically LPBF, in the production of optimized optical components with enhanced structural properties need to be evaluated. This study contributes to the advancement of materials and manufacturing methods for space-based optical instruments, ultimately improving their performance and reliability (Eberle *et al.*, 2018 - 2018).

2. Processing Study

2.1. Parameter Development

For the parameter study, an Aconity Mini LPBF lab machine equipped with a high temperature module was used. To utilize a bigger build chamber within the project the developed process was transferred to an industrial machine with a similar configuration. Therefore a Renishaw AM400HT was used. The general specifications of the used machines are shown in Table 1.

Table 1. Used machine and powder for parameter study.

	Lab Machine - Aconity Mini	**Industrial Machine – Renishaw AM400HT**
Property	• Ytterbium fiber laser (λ=1064 nm) • Pseudo pulsed mode • Laser power: 200 W • Chamber size: Ø98 x 130 mm³ • Protection gas: Ar • Preheating up to 800 °C	• Ytterbium fiber laser (λ=1064 nm) • Pseudo pulsed mode • Laser power: 400 W • Chamber size: 250 x 250 x 300 mm³ • Protection gas: Ar • Preheating up to 500 °C
Powder description	AlSi40	AlSi40
Particle fraction size	20-63 µm	20-63 µm

In the first iteration of the parameter development, an existing parameter set was used from the previous processing of the material on the industrial machine Renishaw AM250 in the preceding project as baseline for the investigations (Müller *et al.*, 2019).

The major adjustment within these studies focuses on the influence of the preheating of the substrate and the altering of the scanning speed for increased productivity on the build quality. The target of this optimization is the realization of a stable process with a low and uniformly distributed porosity. Therefore, for the first trials, the prepared build jobs contained density cubes with a xyz-dimension of 10 x 15 x 10 mm³ for metallographic investigations and cylindrical samples with the xyz-dimensions Ø10 x 15 mm³ for CT measurements to ensure the uniform quality of the build-up material.

The investigated parameter field was derived from the already stated parameter set from the preceding project and altered to achieve higher productivity by changing the scan velocity and the connected parameters point distance and jumping time. The first trial was conducted with a substrate preheating of 500 °C, which is rather close to the melting point of aluminum at 660 °C. This might have affected the melt pool viscosity, which resulted in pores in the lower layers close to the substrate. Therefore, all following experiments were performed using a substrate preheating temperature of 400 °C. The results of the first trials with 500 °C already delivered acceptable results regarding the overall density but exhibited defect accumulations in the bottom part of the specimens (see Fig. 1).

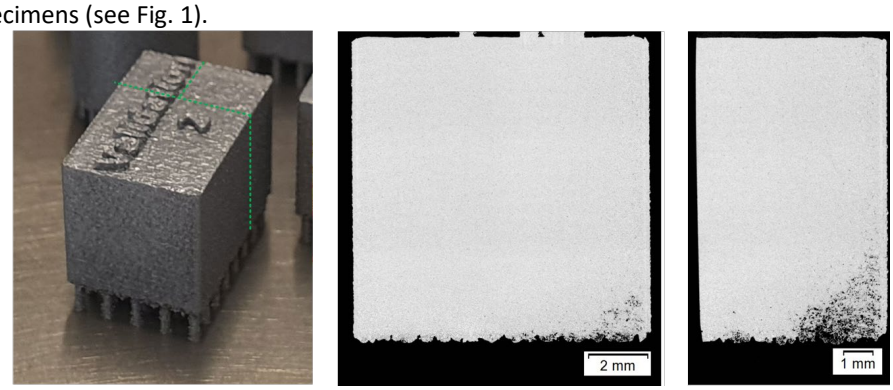

Fig. 1. Results of the first trials with defects in the lower areas.

As described above, the applied preheating temperature of 500 °C was rather close to the melting point of aluminum and thus might have affected the melt pool behavior. Moreover, the low thermal gradient between the solidifying material and the substrate plate might have led to insufficient heat dissipation. To solve this issue, the preheating temperature was lowered to 400 °C and the support structures were re-designed to facilitate a faster heat transport.

Although some spherical gas pores are still visible, the reduction in preheating temperature led to a significantly more homogeneous result in terms of pore distribution. The microstructure consists of primary Si particles in an α-aluminum matrix. The occurrence of the α-aluminium matrix phase compared to the eutectic aluminum-silicon equilibrium phase is favoured by the high cooling rates which occur in the LPBF process. A thorough investigation of the microstructural composition has been performed in the previous project (Nikolaevich Grigoriev *et al.*, 2014; Müller *et al.*, 2019).

This baseline parameter was transferred to the industrial machine AM400HT. It has to be considered that while the Aconity Mini allows the direct control of the scan speed, the AM400HT requires a separate adjustment of the point distance and the jumping time to achieve an equivalent scan speed. The parameter validation consisted of the manufacturing of density cubes, the analysis of the microstructure and the subsequent slight alteration of the process parameters to cope with slight deviations of the results like small dispersed residual pores (see Fig. 1). This behaviour might be caused by differences between the Aconity Mini and the AM400HT, like the longer laser travel distance or the general process control.

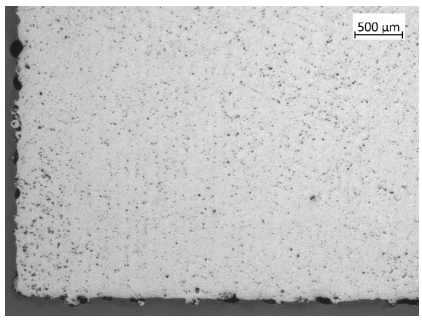

Fig. 2. Metallographic cross section of the validation density cubes.

To reduce the residual porosity, the scan speed was adjusted. For this purpose, density cubes with a varied jumping time between 30 and 52 µs were manufactured to assess a more suitable parameter set with less residual porosity. As a result, an optimal jump time of 30 µm was identified based on metallographic cross-sections (see Table 1) for final parameter sets of lab machine and industrial machine). The faster scan speed decreases the induced energy density and therefore decreases the formation of the observed keyhole pores.

Table 2. Comparison of the parameter sets from the lab machine and the industrial machine with altered jumping time (green) and the resulting reduced volumetric energy density and increased scanning speed.

Machine	**Laser power P_{laser} in W**	**Hatch distance d_{hatch} in µm**	**Volumetric energy density E_v in J/mm³**	**Scanning speed V_{scan} in mm/s**
Lab Machine	200	102	51	1527
Industrial Machine	200	102	41	1933

The altered parameter was validated with the manufacturing of an additional density cubes. The validation samples showed a relative density 99.3% (see Fig. 1).

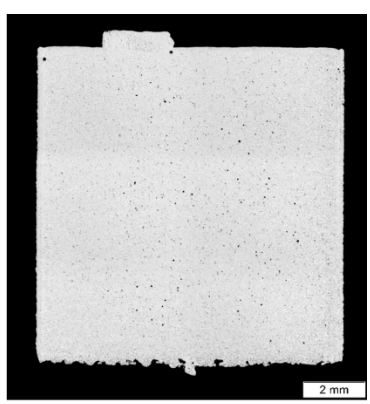

Fig. 3. Density validation cube for the altered parameter set.

2.2. Mechanical Characterization

For the mechanical characterization of the developed parameter sets were characterized via conventional tensile test and the compression testing of two types of lattice cubes. This is done on both the lab machine and industrial machine. The two lattice cubes sample geometries consist of a simple cuboid unit cell and a face centered unit cell with diagonal struts (see Fig. 1). These both are candidates for the final application as inner lattice structure for the mirror application.

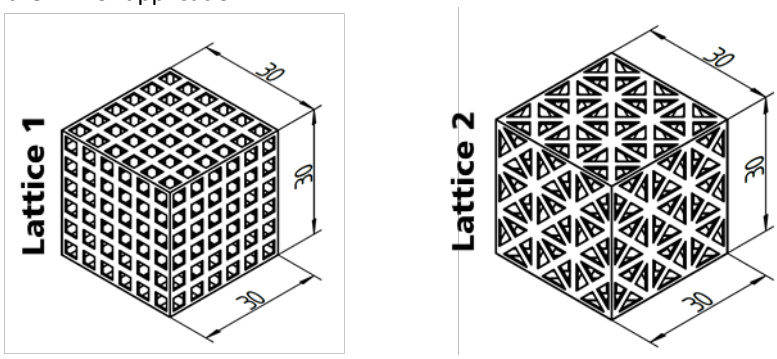

Fig. 4. Visualization of sample dimension for compression testing.

For the characterization of mechanical properties and validation of the industrial transfer, tensile samples on the lab machine and industrial machine were manufactured, turned and tested according to ISO 6892-1. The geometry of the samples was chosen according to DIN 50125-B6x20 and altered by a lower testing diameter to 3 mm to ensure the cracking within the testing length. On the lab machine only the vertical build-up direction was investigated, while on the industrial machine allowed the manufacturing of several build direction. A comparison of the acquired values to tabled values for conventionally manufactured AlSi40 is shown in Tab. 1.

Table 3. Comparison of mechanical properties for conventionally manufactured AlSi40 and for the lab machine and industrial machine.

		Young's Modulus in GPa	**YS in MPa**	**UTS in MPa**	**E in %**
Tabled		102	155	225	1,5
Lab Machine	V	76 ± 12	153 ± 6	222 ± 7	0,8 ± 1,4
Industrial Machine	V	103 ± 7	143 ± 5	200 ± 9	0,7 ± 0,2
	H	96 ± 11	135 ± 4	202 ± 5	1,0 ± 0,1
	D	102 ± 12	140 ± 6	210 ± 3	0,9 ± 0,1

In comparison with the achieved values on the lab machine the tensile strength of the industrial machine samples show a slightly lower value which is within the tabled values for the raw material. The elongation at break is also in similar ranges. In many of the samples, failure occurred in the thread or in the transition area to the gauge length instead of within the gauge length. Accordingly, it can be assumed that the material has a higher mechanical strength than could be measured. One possible mitigation strategy would be to increase

the diameter in the thread compared to the sample diameter in the gauge length to provoke failure at the minimum cross-section in the gauge length rather than at the notches of the thread. The root-cause for the slightly lower tensile strength and irregular breaking at the thread is not yet fully understood. The main hypotheses are an increased notch effect by:

- the granularity of the precipitated Si-particles in the Al-matrix caused by a slightly altered optical system (laser on-off transition) and slightly different process parameters,
- formation of surface irregularities during the process due to altered contour parameters or
- unfavorable ratio between diameter in the thread and sample diameter in the measuring length.

Compression testing of the lattice cubes was carried out on a MTS 810 compression testing machine. The post-processing of the interfaces was important for achieving interpretable and reproducible results. Therefore, any residual support structures were carefully removed manually with a file. Thus, flat contact surfaces could be created for the compression test.

A set of cameras was used to capture occurring deformations during the test. Subsequently, a two-dimensional digital image correlation (DIC) was performed. Seven samples of each lattice type were characterized in compression tests both with and without NiP coating (performed at external service provider), respectively. Failure mainly occurred within the side areas of the lattice cubes.

The results show a significant improvement of the respective compression strengths of each lattice type by almost 200 % after NiP coating. Apparently, the NiP coating dramatically enhanced the stiffness of the lattice structures. Moreover, the coating might have covered some of the surface irregularities (roughness, attached particles) which otherwise might have acted as crack-initiating defects.The compression samples manufactured at the industrial machine exhibit a slightly lower compression strength compared to the previous tested samples, while the elastic stiffness is only slightly reduced. Especially the target lattice structure Lattice 1 shows very similar stiffness values (see Tab. 4 and Fig. 1).

Table 4. Results of the compression testing including the lab-level and industrial level samples.

	ΔL at $F_{Comp.max}$ in mm	**Global Elongation at $F_{Comp.max}$ in %**	**Strength in N/mm²**	**Elastic Stiffness[*] in kN/mm**
Lattice 1	1.52	5.08	126.31	36.16
Lattice 1 – NiP	1.01	3.35	235.38	57.23
Lattice 2	0.65	2.17	77.50	29.50
Lattice 2 – NiP	0.80	2.67	158.37	44.12
Lattice 1 – Industrial Machine	1.14	3.80	91.87	33.86
Lattice 2 – Industrial Machine	0.75	2.49	61.79	21.85

[*] The stiffnesses are to be considered as approximations.

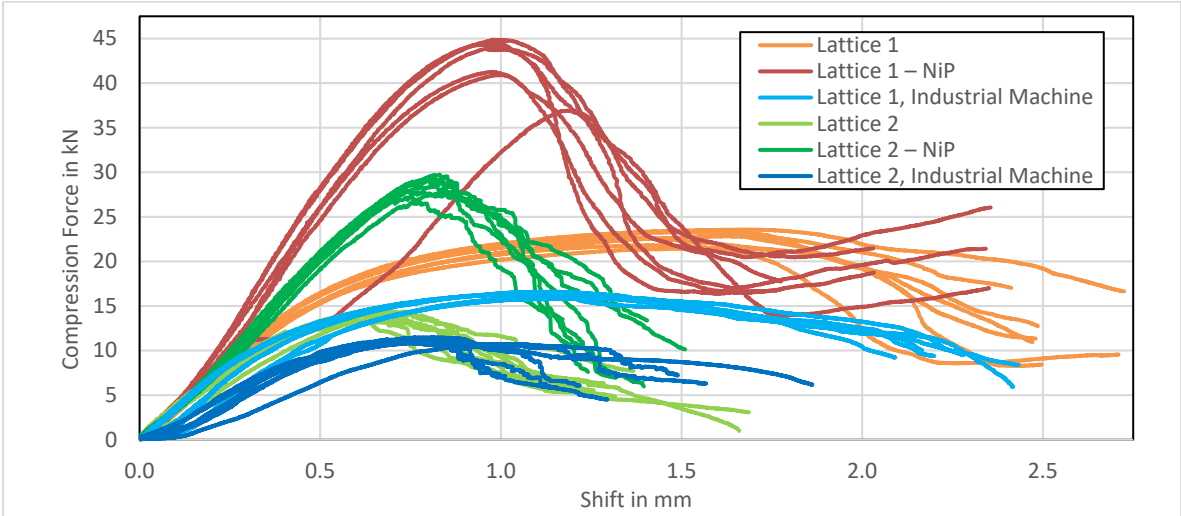

Fig. 5. Results of the compression testing including the lab-level and industrial level samples.

The root cause for the different results cannot be explained sufficiently. The most plausible explanation at the moment lies within a different sharpness and roughness at the corners of struts. A deviating transition there lead to higher local stresses and therefore to earlier failure of the lattice cubes. To confirm this hypothesis CT-scans of the lab and industrial machine lattice cubes were compared at the corner regions of the struts (see Fig. 1). Within this investigation a difference between both samples regarding the slightly smaller struts and higher amount of surface irregularities of the industrial machine manufactured sample is observable.

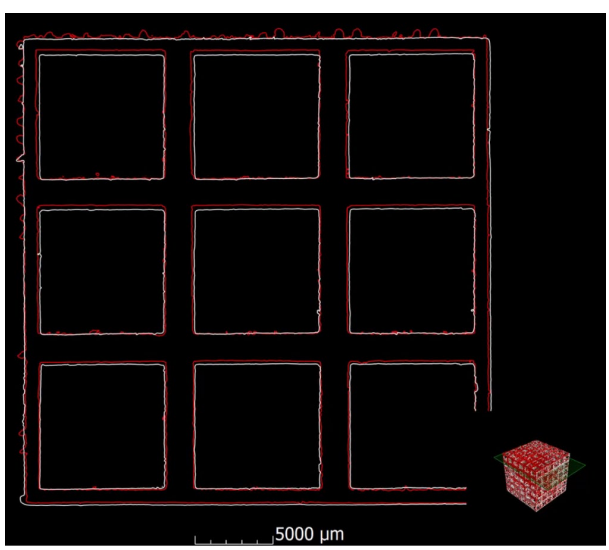

Fig. 6. Comparison of the CT scans of lab (white) and industrial (red) machine lattice 1.

A representative direct image correlation (DIC) of a lattice cubes for each condition (see Fig. 1) provides insight into the behavior of the lattices under compressive load. The uncoated specimens show overall higher van Mises strains, whereas for the coated samples, the highest strains are in the areas of failure.

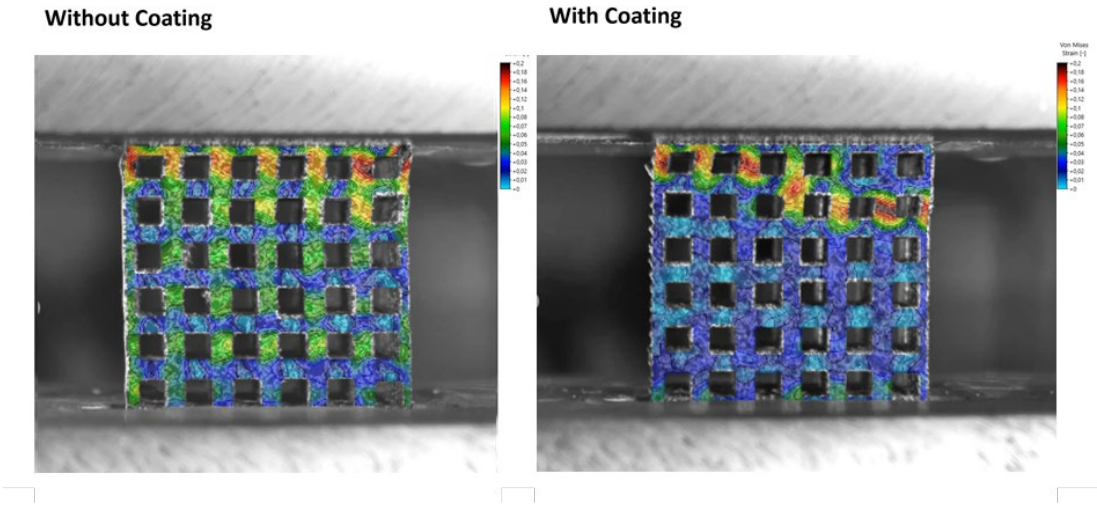

Fig. 7. DIC of lattice type 1 without and with NiP coating during compression testing.

2.3. Demonstrator Manufacturing

To show the capabilities of the LPBF-process of the application target for optical mirrors smaller demonstrator in form of a subcomponent was processed within the planned process chain (see Fig. 8).

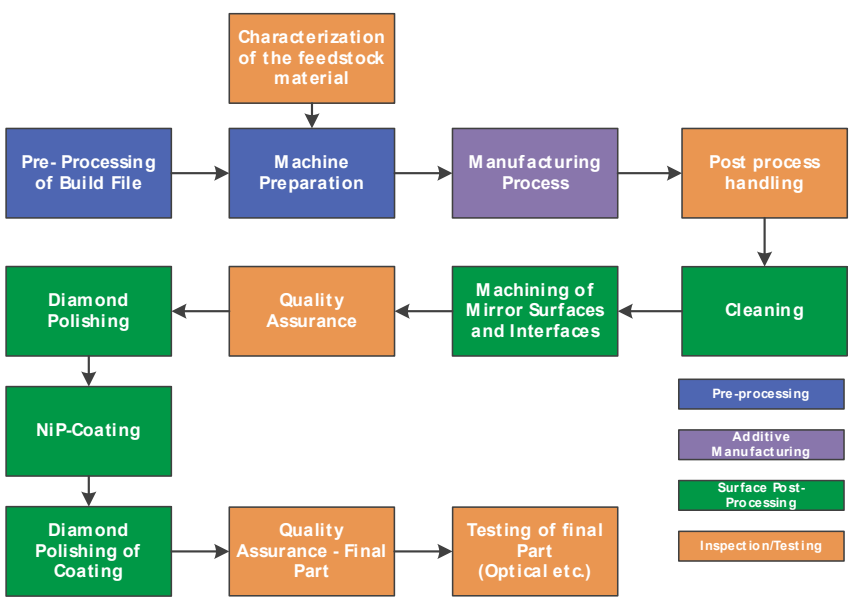

Fig. 8. Process chain for the manufacturing of the subcomponent.

The part is mainly built through an automated process with minimal supervision. Monitoring machine parameters like oxygen level, temperature, and powder dosing ensures success. Excessive oxygen triggers inert gas addition, causing a brief pause. Substrate temperature remains constant at 400°C during the build. After manufacturing, the part is carefully separated from the substrate using clipping and cutting. Mechanical post-processing involves custom clamping, milling, and surface processing. CT scanning confirms no detectable porosity, and ultrasonic cleaning removes residual powder. Vibration-related defects are prevented during cleaning.

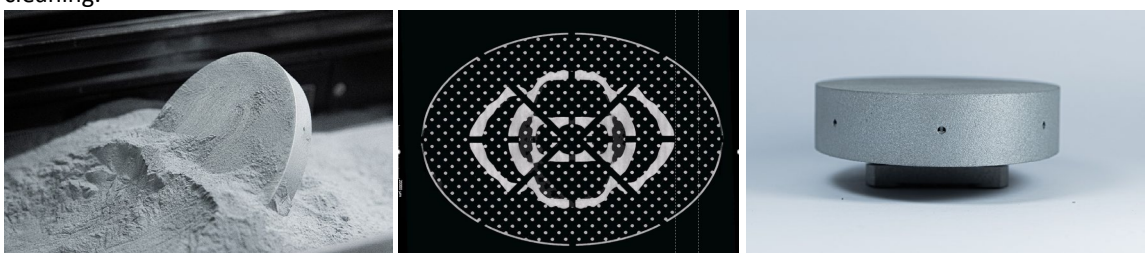

Fig. 9. Manufacturing of Subcomponent, in powder bed (left), in NDI via CT (middle), as built ready for further processing (right).

3. Results and Discussion

The objective of the industrial transfer was to transfer the achieved manufacturing performance on the Aconity Mini to the Renishaw AM400HT. Verification of this process was divided into:

- Material properties: Material properties shall be the same / similar
- Manufacturing feasibility

The transfer of the developed process chain to an industrial machine with regards to material properties can be evaluated as successful. Minor setbacks regarding mechanical performance, which might be caused by:

- Microstructure,
- Geometrical differences (notch effect) and/or
- Surface morphology/ roughness

offer potential for future adjustments of the process, but at the current stage the process is suitable for manufacturing of the PAM-demonstrator. The transferring the process chain to other machines with bigger volumes but other optical system needs more adjustments.

In conclusion the transfer to an industrial machine can be considered successful and suitable for further processing of AlSi40 for the mirror application. Even though some valuable learnings can be derived from the transfer. Even a one-to-one transfer of a parameter set developed on one machine to a non-identical machine with similar configuration (technological, optical, process control) is not possible without changes in some parameters. As shown a minor increase in scan speed was needed to get dense material similar to the developed parameter set on the lab machine. So minor differences can lead to a limited reproducibility on another machine. The effect on reproducibility is even bigger when the configurations changes more drastically, like different laser systems or spot-sizes. Therefore it is advised to always validate existing parameter sets when transferring them between machines.

References

Eberle, S., Reutlinger, A., Curzadd, B., Mueller, M., Riede, M., Wilsnack, C., Brandão, A., Pambaguian, L., Seidel, A., López, E., Brueckner, F., Beyer, E. and Leyens, C. (2018 - 2018), "Additive manufacturing of an AlSi40 mirror coated with electroless nickel for cryogenic space applications", in Karafolas, N., Sodnik, Z. and Cugny, B. (Eds.), International Conference on Space Optics — ICSO 2018, Chania, Greece, 10/9/2018 - 10/12/2018, SPIE, p. 40.

Hilpert, E., Hartung, J., Lukowicz, H. von, Herffurth, T. and Heidler, N. (2019), "Design, additive manufacturing, processing, and characterization of metal mirror made of aluminum silicon alloy for space applications", Optical Engineering, Vol. 58 No. 09, p. 1.

Jenzer, S., Alves, M., Delerue, N., Gonnin, A., Grasset, D., Letellier-Cohen, F., Mercier, B., Mistretta, E., Prevost, C., Vion, A. and Wilmes, J.-P. (2017), "Study of the suitability of 3D printing for Ultra-High Vacuum applications", Journal of Physics: Conference Series, Vol. 874, p. 12097.

Ma, P., Prashanth, K., Scudino, S., Jia, Y., Wang, H., Zou, C., Wei, Z. and Eckert, J. (2014), "Influence of Annealing on Mechanical Properties of Al-20Si Processed by Selective Laser Melting", Metals, Vol. 4 No. 1, pp. 28–36.

Müller, M., Mirko, R., Eberle, S., Brandao, A., Pambaguian, L., Lopez, E., Brueckner, F. and Leyens, C. (2019), Fabrication of lightweight optical components made of hypereutectic AlSi40 by means of Additive Manufacturing.

Nikolaevich Grigoriev, S., Vasilievna Tarasova, T., Olegovna Gvozdeva, G. and Nowotny, S. (2014), "Structure Formation of Hypereutectic Al-Si-Alloys Produced by Laser Surface Treatment", Strojniški vestnik – Journal of Mechanical Engineering, Vol. 60 No. 6, pp. 389–394.